RADAR TARGET RECOGNITION BY PROJECTED FEATURES OF FREQUENCY-DIVERSITY RCS

K.-C. Lee, C.-W. Huang, and M.-C. Fang

Department of Systems and Naval Mechatronic Engineering
National Cheng-Kung University
Tainan 701, Taiwan

Abstract—In this paper, the radar target recognition is given by projected features of frequency-diversity RCS (radar cross section). The frequency diversity means signals are collected by sweeping the frequency of the incident illumination. Initially, the frequency-diversity RCS data from targets are collected and projected onto the PCA (principal components analysis) space. The elementary recognition of targets is efficiently performed on the PCA space. To achieve well separate recognition of targets, the features of the PCA space are further projected onto the LDA (linear discriminant algorithm) space. Simulation results show that accurate results of radar target recognition can be obtained by the proposed frequency-diversity scheme. In addition, the proposed frequency-diversity scheme has good ability to tolerate noise effects in radar target recognition.

1. INTRODUCTION

Radar target recognition means to identify the classes of targets by using different types of features. The SAR (synthetic aperture radar) images of targets are good features for radar target recognition. However, it is not easy to obtain such features. In general, the RCS data are easy to obtain and then become good candidates for radar target recognition. In [1, 2], we have successfully utilized angular-diversity RCS (radar cross section) data as the features to identify radar targets. The angular-diversity technique means signals are collected by sweeping the angles in space. Although angular-diversity RCS data theoretically give accurate recognition results in our past studies of [1, 2], they are impractical. Unlike the angular diversity, the frequency-diversity (or frequency-swept) technique collects signals by sweeping the frequency of the incident illumination.

In practical application, the frequency-diversity measurement is easier to implement than that of angular diversity. This then motivates us to develop a frequency-diversity RCS based technique for the radar target recognition.

In this paper, the radar target recognition is given based on projected features of frequency-diversity RCS. Similar to the use of frequency-diversity techniques in microwave imaging [3, 4], the RCS are collected by sweeping the frequency of the incident wave. These frequency-diversity RCS data are then projected onto another eigenspace for target recognition. To achieve efficient recognition, the collected frequency-diversity RCS data (usually high-dimensional) are first projected onto a low-dimensional PCA (principal components analysis) space [5, 6] and the elementary target recognition is performed on the PCA space. To achieve reliable recognition, the projected features on the PCA space are further projected onto the LDA (linear discriminant algorithm) space [5, 6] and well-separate recognition of targets can be obtained on the LDA space. Simulation results show that accurate recognition results are obtained by the proposed frequency-diversity scheme. In addition, our results also show that the proposed frequency-diversity scheme has good ability to tolerate noise effects. The idea of angular or frequency diversity comes from microwave diversity imaging [7, 8] that reconstructs the shape of a target by collecting electric fields of diversity. The diversity techniques of microwave imaging include angular, frequency and polarization diversity. According to the electromagnetic-wave theory, the scattered electric field in the far field is proportional to the spatial Fourier transform of the object function. The use of frequency-diversity measurement can produce data that efficiently fill the Fourier space. The frequency-diversity techniques have been applied to microwave imaging for many years. However, there still exists no study that utilizes such techniques in radar target recognition. To our knowledge, this is the first study that applies frequency-diversity RCS to the radar target recognition.

In Section 2, the formulation of frequency-diversity based radar target recognition is given. Numerical simulation is given in Section 3. Finally, the conclusion is given in Section 4.

2. FORMULATION

The proposed radar recognition algorithm has no limitation on types of targets. Without loss of generality, the targets of simulation are chosen as ships for simplicity. The frequency-diversity RCS data from different types of ships are chosen as features for target recognition.
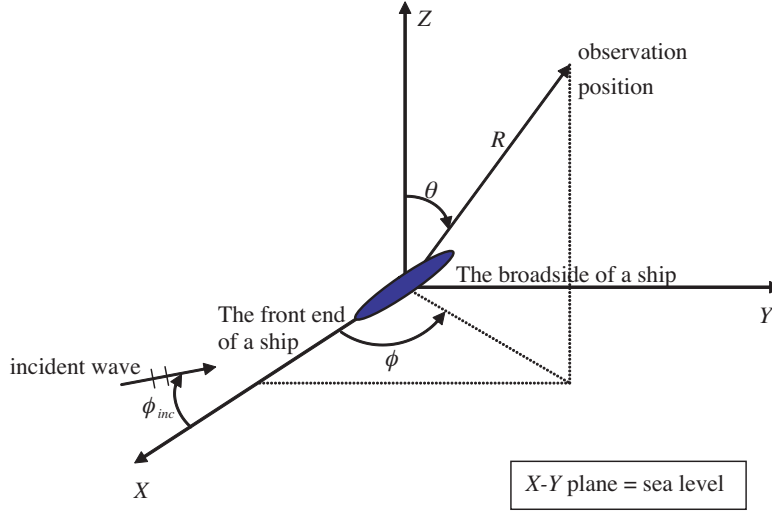
Figure 1. Schematic diagram of a ship illuminated by an incident plane wave.

Consider a ship on the sea level (X-Y plane) illuminated by a plane wave $\overline{E}_i = e^{-j\overline{k}\cdot\overline{r}}\hat{z}$ where $\overline{k}$ is the wavenumber and $\overline{r}$ is the location, as shown in Figure 1. This incident wave propagates horizontally at an angle of ϕ_{inc} with respect to the $-\hat{x}$ direction. The spherical coordinate system is defined as (R, θ, ϕ) where R is the distance from observation position to origin, θ is the elevation angle and ϕ is the azimuth angle. The RCS in the direction of (θ, ϕ) is defined as [9]

$$\text{RCS} = \lim_{R\to\infty} 4\pi R^2 \frac{\left|\overline{E}_s(\theta, \phi)\right|^2}{\left|\overline{E}_i\right|^2}. \tag{1}$$

where $\overline{E}_s(\theta, \phi)$ is the scattered electric field.

The goal is to identify the target by its frequency-diversity RCS. The target is illuminated by incident waves from directions of $\phi_{inc} = 0°$, $90°$ and $180°$, respectively. The frequency-diversity (frequencies are chosen as f_1, f_2, ..., f_{N_f}) RCS data from a ship at a fixed evaluation angle θ are collected to constitute a $(3 \cdot N_f)$ dimensional column vector, as shown in each column of the matrix structure in Figure 2. Assume we have C types of known ships totally, i.e., type #c for $c = 1, 2, \ldots,$ C. By choosing the evaluation angle as θ_1, θ_2, ..., θ_{N_θ} for all types of ships, we have $n_T = N_\theta \cdot C$ column vectors totally (denoted as $\overline{x}_i$, $i = 1, 2, \ldots, n_T$) to constitute the RCS matrix, as shown in the

matrix structure of Figure 2. For simplicity, C is assumed to be 3 in the illustration of Figure 2. The dimensions of the RCS matrix are $(3 \cdot N_f) \times (N_\theta \cdot C)$. The signal processing of target recognition in this study contains two steps, i.e., PCA [5, 6] (the first step) and LDA [5, 6] (the second step), and will be given in the following.

		ship of type #1				ship of type #2				ship of type #3			
		θ_1	θ_2	$\cdots$	θ_{N_θ}	θ_1	θ_2	$\cdots$	θ_{N_θ}	θ_1	θ_2	$\cdots$	θ_{N_θ}
$\phi_{inc}=$ 0^0	f_1	RCS	RCS	$\cdots$	RCS	RCS	RCS	$\cdots$	RCS	RCS	RCS	$\cdots$	RCS
	f_2	RCS	RCS	$\cdots$	RCS	RCS	RCS	$\cdots$	RCS	RCS	RCS	$\cdots$	RCS
	$\vdots$	$\vdots$	$\vdots$	$\cdots$	$\vdots$	$\vdots$	$\vdots$	$\cdots$	$\vdots$	$\vdots$	$\vdots$	$\cdots$	$\vdots$
	f_{N_f}	RCS	RCS	$\cdots$	RCS	RCS	RCS	$\cdots$	RCS	RCS	RCS	$\cdots$	RCS
$\phi_{inc}=$ 90^0	f_1	RCS	RCS	$\cdots$	RCS	RCS	RCS	$\cdots$	RCS	RCS	RCS	$\cdots$	RCS
	f_2	RCS	RCS	$\cdots$	RCS	RCS	RCS	$\cdots$	RCS	RCS	RCS	$\cdots$	RCS
	$\vdots$	$\vdots$	$\vdots$	$\cdots$	$\vdots$	$\vdots$	$\vdots$	$\cdots$	$\vdots$	$\vdots$	$\vdots$	$\cdots$	$\vdots$
	f_{N_f}	RCS	RCS	$\cdots$	RCS	RCS	RCS	$\cdots$	RCS	RCS	RCS	$\cdots$	RCS
$\phi_{inc}=$ 180^0	f_1	RCS	RCS	$\cdots$	RCS	RCS	RCS	$\cdots$	RCS	RCS	RCS	$\cdots$	RCS
	f_2	RCS	RCS	$\cdots$	RCS	RCS	RCS	$\cdots$	RCS	RCS	RCS	$\cdots$	RCS
	$\vdots$	$\vdots$	$\vdots$	$\cdots$	$\vdots$	$\vdots$	$\vdots$	$\cdots$	$\vdots$	$\vdots$	$\vdots$	$\cdots$	$\vdots$
	f_{N_f}	RCS	RCS	$\cdots$	RCS	RCS	RCS	$\cdots$	RCS	RCS	RCS	$\cdots$	RCS

Figure 2. Illustration of the frequency-diversity RCS matrix.

In the first step of recognition, the PCA is utilized. The mean vector $\overline{m}^{(x)}$ of the total n_T training vectors is given as

$$\overline{m}^{(x)} = \frac{1}{n_T} \sum_{i=1}^{n_T} \overline{x}_i. \tag{2}$$

The centered vector $\overline{\Phi}_i$ for the column vector $\overline{x}_i$ is given as

$$\overline{\Phi}_i = \overline{x}_i - \overline{m}^{(x)}, \quad i = 1, 2, \ldots, n_T. \tag{3}$$

The covariance matrix $\overline{\overline{\Sigma}}$ is defined as

$$\overline{\overline{\Sigma}} = \frac{1}{n_T} \left(\overline{\Phi}_1, \overline{\Phi}_2, \ldots, \overline{\Phi}_{n_T} \right) \cdot \left(\overline{\Phi}_1, \overline{\Phi}_2, \ldots, \overline{\Phi}_{n_T} \right)^T \tag{4}$$

where "T" denotes the transpose. The dimensions of $\overline{\overline{\Sigma}}$ are $(3 \cdot N_f) \times (3 \cdot N_f)$. Assume that λ_i, $i = 1, 2, \ldots, n_{PCA}$ are the largest n_{PCA}

eigenvalues and $\overline{v}_i$, $i = 1, \ldots, n_{PCA}$ are their normalized eigenvectors. These eigenvectors will constitute an n_{PCA}-dimensional PCA space. Each column vector $\overline{x}_i$ of the RCS matrix is projected onto the PCA space to obtain a new vector $\overline{y}_i$ (n_{PCA}-dimensional). The result is

$$\overline{y}_i = \overline{\overline{P}} \cdot \left(\overline{x}_i - \overline{m}^{(x)} \right), \ i = 1, 2, \ldots, n_T \tag{5}$$

where

$$\overline{\overline{P}} = \left(\overline{v}_1 \ \overline{v}_2 \ \ldots \ \overline{v}_{n_{PCA}} \right)^T. \tag{6}$$

In general, we have $n_{PCA} \ll (3 \cdot N_f)$. In other words, the dimensions of the RCS feature are greatly reduced by (6). The mean (or class center) for features of the type #c target on the PCA space is given by

$$\overline{m}_c^{(y)} = \frac{1}{N_\theta} \sum_{i=(c-1) \cdot N_\theta}^{c \cdot N_\theta} \overline{y}_i, \quad c = 1, 2, \ldots, C. \tag{7}$$

For an unknown target, its frequency-diversity RCS at a given elevation angle θ are collected to constitute an RCS vector $\overline{x}$. This column vector $\overline{x}$ is projected onto the PCA space according to (5)–(6) and the result is $\overline{y}$. The distance, i.e., class error, of this measurement with respect to the known target of type #c is given by

$$d_c = \left\| \overline{y} - \overline{m}_c^{(y)} \right\|, \quad c = 1, \ldots, C. \tag{8}$$

Therefore, we can define the "*similarity*" with respect to the known target of type #c as

$$similarity = 1 - \frac{d_c}{\sum\limits_{c=1}^{C} d_c}, \quad c = 1, \ldots, C. \tag{9}$$

Obviously, we have $0 < similarity < 1$. The value of *similarity* is proportional to the degree of similarity. The largest *similarity* means the unknown target has the most similarity to this type of known ship. In the second step, the projection of the first step is further projected onto the LDA space. It should be noted that the goal of this step is to find a projection that can well separate features of different classes. Initially, the within-class scatter matrix $\overline{\overline{S}}_W$ is defined as

$$\overline{\overline{S}}_W = \sum_{i=1}^{n_T} \left[\left(\overline{y}_i - \overline{m}_c^{(y)} \right) \cdot \left(\overline{y}_i - \overline{m}_c^{(y)} \right)^T \right] \tag{10}$$

and the between-class scatter matrix $\overline{\overline{S}}_B$ is defined as

$$\overline{\overline{S}}_B = \sum_{c=1}^{C} \left[n_c \left(\overline{m}_c^{(y)} - \overline{m}^{(y)} \right) \cdot \left(\overline{m}_c^{(y)} - \overline{m}^{(y)} \right)^T \right]. \qquad (11)$$

In (11), the $\overline{m}_c^{(y)}$ has been given in (7) and

$$\overline{m}^{(y)} = \frac{1}{n_T} \sum_{i=1}^{n_T} \overline{y}_i. \qquad (12)$$

According to [10, 11], the eigenvectors of $[\overline{\overline{S}}_W]^{-1}\overline{\overline{S}}_B$ will constitute an eigenspace that separates the projected features best. We may choose the largest n_{LDA} eigenvalues and their corresponding eigenvectors to dominate the projection. Therefore, we can project features from the PCA space to the LDA space as

$$\overline{z}_i = \overline{\overline{L}} \cdot \overline{y}_i, \quad i = 1, 2, \ldots, n_T, \qquad (13)$$

where $\overline{\overline{L}}$ is the transformation matrix with its rows composed of the n_{LDA} eigenvectors. The process of target recognition on LDA space is similar to (8)–(9) except that features of PCA space in (8)–(9) are replaced by features of LDA space.

3. NUMERICAL SIMULATION

In this section, numerical examples are given to illustrate the above target recognition algorithm. The RCS data are calculated by the commercial software of Ansoft HFSS. This software has been proved to be accurate by many researchers in electromagnetic waves. Assume there are three types of known ships (i.e., $C = 3$) including type #1 (for modeling the container vessel), type #2 (for modeling the naval ship) and type #3 (for modeling the fishing boat). The geometrical models for these three types of known ships are shown in Figure 3. The dimensions for these three types of ships are chosen to be $k \cdot l_1 = 9.4$, $k \cdot l_2 = 6.3$ and $k \cdot l_3 = 3.1$, where l_c ($c = 1, 2, 3$) denotes the length for the ship of type #c. All ships are on the sea level (X-Y plane) and the characteristic for the surface roughness of sea water is assumed to be sinusoidal as

$$z(x, y) = \frac{4}{75} l_1 \cdot \sin\left(\frac{15\pi}{4}x\right) \sin\left(\frac{15\pi}{4}y\right) + \frac{8}{75} l_1. \qquad (14)$$

The sea water has dielectric constant $\varepsilon_r = 81$ and conductivity $\sigma = 4\,\mathrm{S/m}$. The RCS from all types of known ships are collected to
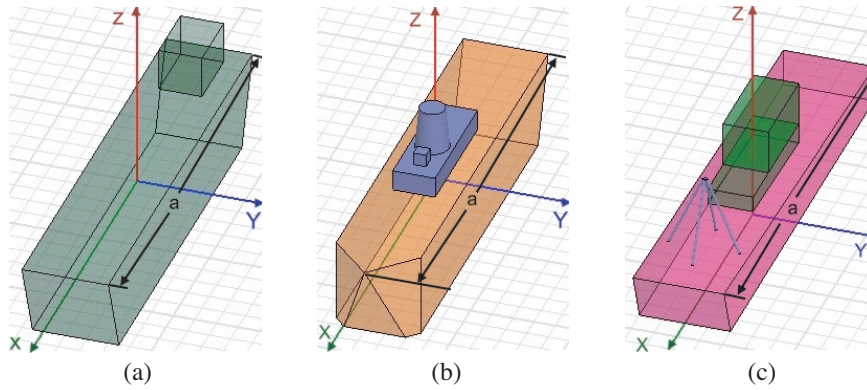
Figure 3. Geometrical models for the three types of known ships: (a) type #1, (b) type #2 and (c) type #3.

constitute a frequency-diversity RCS matrix as the matrix structure of Figure 2. In the learning phase, the RCS matrix in Figure 2 is obtained by choosing the evaluation angles to be $\theta_1 = 61°$, $\theta_2 = 63°$, ..., $\theta_{N_\theta} = 89°$ and the frequencies to be $f_1 = 3.0\,\text{GHz}$, $f_2 = 3.1\,\text{GHz}$, ..., $f_{N_f} = 3.9\,\text{GHz}$. Therefore, we have $N_\theta = 15$ and $N_f = 10$, and the dimensions of the RCS matrix are 30×45.

In the testing phase, the frequency-diversity RCS data from the unknown target at a given evaluation angle θ are collected to constitute a column vector. In the first example, the testing target (unknown) is assumed to be the ship of type #1. We will utilize the frequency-diversity RCS data to decide which type of known ships resembles the unknown target most. In our simulation, the testing evaluation angles are chosen as $\theta = 62°$, $64°$, ..., and $90°$, respectively. That is, the target is tested 15 times. Figure 4 shows the similarity with respect to each type of known ship at different testing evaluation angle of θ. Note that the highest plot at a given θ means this type of known ship has the most similarity to the testing target. In Figure 4(a), only the PCA (i.e., the first step of Section 2) is utilized. The frequency-diversity RCS data are projected onto the 2-dimensional PCA space. In Figure 4(b), both the PCA and LDA (i.e., both the first and second steps of Section 2) are utilized. The frequency-diversity RCS data are projected onto the 3-dimensional PCA space, and then to the 2-dimensional LDA space. Figure 4(a) and Figure 4(b) show that the known ship of type #1 resembles the unknown target best. The recognition results are correct at all the 15 testing evaluation angles and the successful recognition rate is $15/15 = 100\%$. The discrimination for the highest plot (i.e., difference between the highest plot and other plots) of Figure 4(b) is
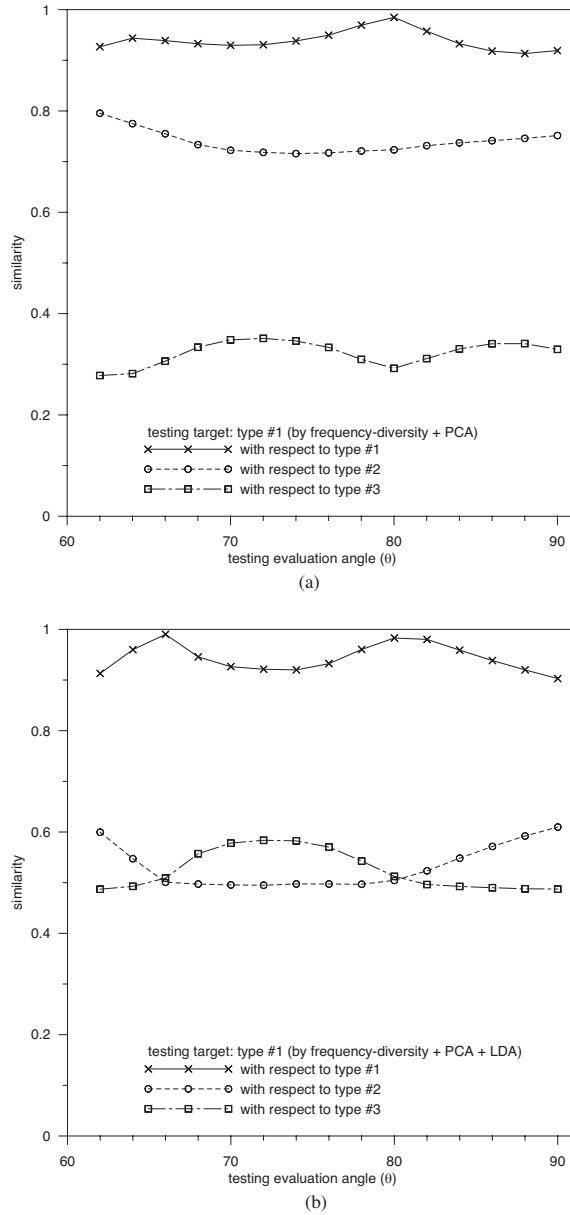
Figure 4. Similarity with respect to each type of known ship at different testing evaluation angles of θ as the testing target is the ship of type #1. The RCS data are projected (a) onto the 2-dimensional PCA space, and (b) onto the 3-dimensional PCA space and then to the 2-dimensional LDA space.
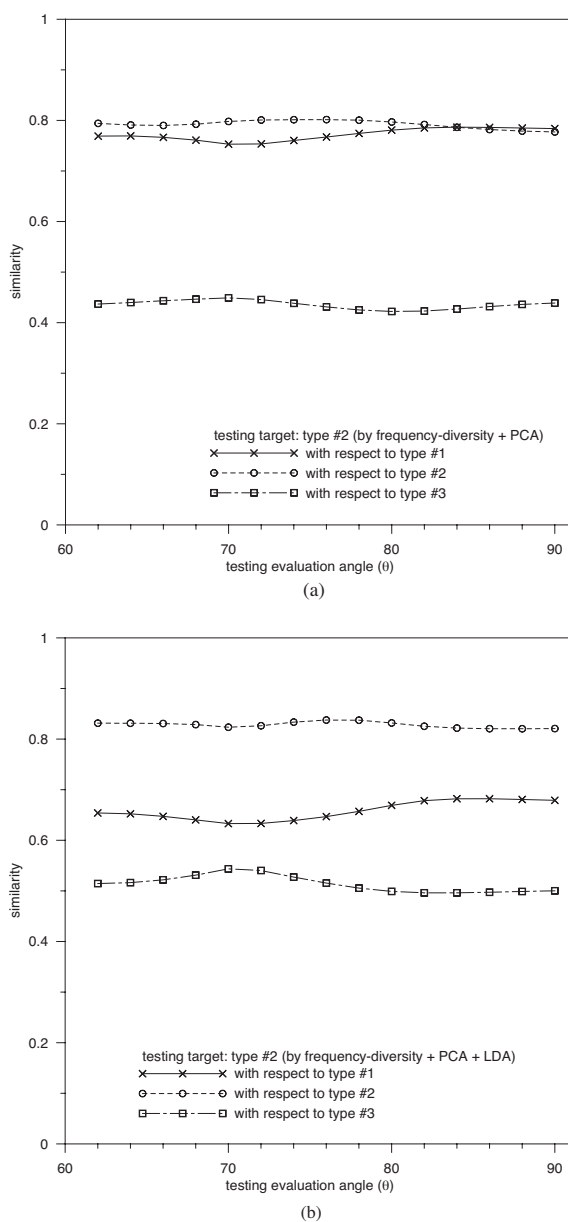
Figure 5. Similarity with respect to each type of known ship at different testing evaluation angles of θ as the testing target is the ship of type #2. The RCS data are projected (a) onto the 2-dimensional PCA space, and (b) onto the 3-dimensional PCA space and then to the 2-dimensional LDA space.
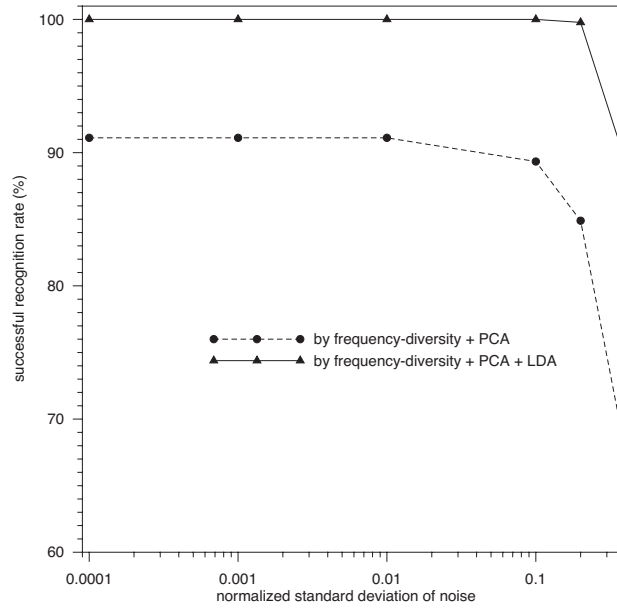
Figure 6. The mean of successful recognition rate with respect to noise levels with the frequency-diversity RCS treated by only PCA, or by PCA and then LDA.

better than that of Figure 4(a).

In the second example, the testing target (unknown) is assumed to be the ship of type #2. All the recognition procedures are the same as those of the previous example. Figure 5(a) shows the recognition results by projecting the frequency-diversity RCS data onto the 2-dimensional PCA space. It shows that the discrimination for the highest plot of Figure 5(a) is very poor. The recognition results are even wrong at the testing evaluation angles of $\theta = 84°$, $86°$, $88°$, $90°$. The successful recognition rate is $11/15 = 73.3\%$. Figure 5(b) shows the recognition results by projecting the frequency-diversity RCS data onto the 3-dimensional PCA space, and then to the 2-dimensional LDA space. It shows that the discrimination for the highest plot is greatly improved. From Figure 5(b), it shows that the known ship of type #2 resembles the unknown target best. The recognition results are correct at all the 15 testing evaluation angles and the successful recognition rate is $15/15 = 100\%$.

To understand the effects of noise, each RCS is added by a quantity of independent random numbers having a Gaussian distribution with zero mean. The standard derivation of noise is normalized by the root-

mean square value of the RCS. The standard derivations of applied noises include 10^{-4}, 10^{-3}, 10^{-2}, 10^{-1}, 2×10^{-1} and 4×10^{-1}. Figure 6 shows the mean of successful recognition rate with the noisy frequency-diversity RCS treated by PCA, or by PCA and then LDA. The dimensions of the projected PCA and LDA space are the same as those given in the previous two examples. From Figure 6, it shows that fair recognition rate can be achieved with the noisy frequency-diversity RCS treated by only PCA. As the noisy frequency-diversity RCS data are further treated by LDA, the mean of successful recognition rate will be greatly improved. The goal of this example is to illustrate that our frequency-diversity recognition algorithm can tolerate noise effects.

The above numerical simulation (including the Ansoft HFSS software) is executed using the personal computer with Pentium-3.0 CPU. The computer programs are coded using the Matlab-7.

4. CONCLUSION

In this paper, the radar target recognition is given by projected features of frequency-diversity RCS. The frequency-diversity RCS data from targets are first processed by PCA, and then further treated by LDA. Our results show that accurate recognition results can be obtained by the proposed frequency-diversity scheme. In addition, the proposed frequency-diversity scheme can tolerate noise effects in the radar target recognition. Although the targets of simulation are somewhat simple, they do not affect the contribution of this study. Because the main goal of this paper is to show that projected features of frequency-diversity RCS can well identify radar targets even though there exist measured noises. From physical points of views, the RCS based recognition of radar targets is basically an approximate approach of inverse scattering [12–23]. Since frequency-diversity techniques are successful in inverse scattering, they must contain much information about targets. Therefore, it is reasonable that the frequency diversity based techniques have good performance in the radar target recognition of this study.

REFERENCES

1. Lee, K. C., J. S. Ou, and C. H. Huang, "Angular-diversity radar recognition of 12 ships by transformation based approaches — Including noise effects," *Progress In Electromagnetic Research*, PIER 72, 145–158, 2007.

2. Lee, K. C. and J. S. Ou, "Radar target recognition by using linear discriminant algorithm on angular-diversity RCS," *Journal of Electromagnetic Waves and Applications*, Vol. 21, No. 14, 2033–2048, 2007.

3. Farhat, N. H., T. Dzekov, and E. Ledet, "Computer simulation of frequency swept imaging," *Proceedings of the IEEE*, Vol. 64, No. 9, 1453–1454, 1976.

4. Chi, C. and N. H. Farhat, "Frequency swept tomographic imaging of three-dimensional perfectly conducting objects," *IEEE Transactions on Antennas and Propagation*, Vol. 29, No. 2, 312–319, 1981.

5. Moon, T. K. and W. C. Stirling, *Mathematical Methods and Algorithms for Signal Processing*, Prentice Hall, 2000.

6. Duda, R. O., P. E. Hart, and D. G. Stork, *Pattern Classification*, 2nd edition, John Wiley & Sons Inc., 2001.

7. Farhat, N. H., "Microwave diversity imaging and automated target identification based on models of neural networks," *IEEE Proceedings*, Vol. 77, No. 5, 670–681, 1989.

8. Lee, K. C., "Polarization effects on bistatic microwave imaging of perfectly conducting cylinders," Master Thesis, National Taiwan University, Taipei, Taiwan, 1991.

9. Ruck, G. T., D. E. Barrick, W. D. Stuart, and C. K. Krichbaum, *Radar Cross Section Handbook*, Vol. 1, Plenum, New York, 1970.

10. Fisher, R. A., "The statistical utilization of multiple measurements," *Annals of Eugenics*, Vol. 8, 376–386, 1938.

11. Wilks, S. S., *Mathematical Statistics*, Wiley, New York, 1963.

12. Oka, S., H. Togo, N. Kukutsu, and T. Nagatsuma, "Latest trends in millimeter-wave imaging technology," *Progress In Electromagnetics Research Letters*, Vol. 1, 197–204, 2008.

13. Capineri, L., D. Daniels, P. Falorni, O. Lopera, and C. Windsor, "Estimation of relative permittivity of shallow soils by using the ground penetrating radar response from different buried targets," *Progress In Electromagnetics Research Letters*, Vol. 2, 63–71, 2008.

14. Zainud-Deen, S. H., W. M. Hassen, E. M. Ali, and K. H. Awadalla, "Breast cancer detection using a hybrid finite difference frequency

domain and particle swarm optimization techniques," *Progress In Electromagnetics Research B*, Vol. 3, 35–46, 2008.

15. Makki, S. V., T. Z. Ershadi, and M. S. Abrishamian, "Determining the specific ground conductivity aided by the horizontal electric dipole antenna near the ground surface," *Progress In Electromagnetics Research B*, Vol. 1, 43–65, 2008.

16. Zhou, Q., Y.-J. Xie, and Z. Chen, "Prediction of equipment-to-equipment coupling through antennas mounted on an aircraft," *Journal of Electromagnetic Waves and Applications*, Vol. 21, No. 5, 653–663, 2007.

17. Huang, C.-H., Y.-F. Chen, and C.-C. Chiu, "Permittivity distribution reconstruction of dielectric objects by a cascaded method," *Journal of Electromagnetic Waves and Applications*, Vol. 21, No. 2, 145–159, 2007.

18. Zhong, X.-M., C. Liao, W. Chen, Z.-B. Yang, Y. Liao, and F.-B. Meng, "Image reconstruction of arbitrary cross section conducting cylinder using UWB pulse," *Journal of Electromagnetic Waves and Applications*, Vol. 21, No. 1, 25–34, 2007.

19. Yu, G. and T. J. Cui, "Image and localization properties of LHM superlens excited by 3D horizontal electric dipoles," *Journal of Electromagnetic Waves and Applications*, Vol. 21, No. 1, 35–46, 2007.

20. Chen, X., D. Liang, and K. Huang, "Microwave imaging 3-D buried objects using parallel genetic algorithm combined with FDTD technique," *Journal of Electromagnetic Waves and Applications*, Vol. 20, No. 13, 1761–1774, 2006.

21. Zacharopoulos, A., S. R. Arridge, O. Dorn, V. Kolehmainen, and J. Sikora, "3D shape reconstruction in optical tomography using spherical harmonics and bem," *Journal of Electromagnetic Waves and Applications*, Vol. 20, No. 13, 1827–1836, 2006.

22. Semenov, S. Y., V. G. Posukh, Y. E. Sizov, A. E. Bulyshev, A. Souvorov, A. Nazarov, T. C. Williams, and P. N. Repin, "Microwave tomographic imaging of the heart in intact swine," *Journal of Electromagnetic Waves and Applications*, Vol. 20, No. 7, 873–890, 2006.

23. Guo, B., Y. Wang, J. Li, P. Stoica, and R. Wu, "Microwave imaging via adaptive beamforming methods for breast cancer detection," *Journal of Electromagnetic Waves and Applications*, Vol. 20, No. 1, 53–63, 2006.